Journal of Zhejiang University SCIENCE A
ISSN 1673-565X (Print); ISSN 1862-1775 (Online)
www.zju.edu.cn/jzus; www.springerlink.com
E-mail: jzus@zju.edu.cn

Penetration of disk fragments following impact on thin plate*

Juan-juan LI[1], Hai-jun XUAN[†‡1], Lian-fang LIAO[2], Wei-rong HONG[1], Rong-ren WU[1]

([1]*Insititute of Chemical Machinery, Zhejiang University, Hangzhou 310027, China*)

([2]*Shenyang Aeroengine Research Institute, Shenyang 110015, China*)

[†]E-mail: marine@zju.edu.cn

Received Oct. 24, 2008; Revision accepted Dec. 2, 2008; Crosschecked Apr. 23, 2009

Abstract: To investigate the ballistic resistance and failure pattern of aeroengine casing following the impact of disk fragments, and to determine the optimum case structure, the phenomena of a 1/3rd disk fragment impact on single and double-layered thin plate targets were simulated using nonlinear dynamical analysis software MSC.Dytran. Strain rate effect was introduced in a Johnson-Cook (JC) material model for the disk fragment and the plate. Impact modeling was based on the Arbitrary Lagrange-Eulerian method, and simulated using explicit finite element method (FEM). Simulation results showed that the major failure pattern of the plate is shearing and tensile fracture with large plastic deformation. It was also concluded that the ballistic limit velocity increases with the standoff distance when it is beyond a certain value, and that greater resistance is obtained when the front plate has either a proportionately low or high thickness. The impact resistance of a double-layered plate may exceed that of a single plate if the thicknesses and standoff distance of the two plates are set appropriately.

Key words: Aeroengine, Disk burst failure, Case containment capability, Ballistic limit velocity
doi:10.1631/jzus.A0820746 **Document code:** A **CLC number:** TH/C3778

INTRODUCTION

A major hazard in modern aviation is the failure of an aeroengine fan, compressor or turbine disk during high speed rotation. Low cycle fatigue, material fault, faulty assembly, and other factors may directly cause disk burst under operating conditions. A catastrophic burst accident could also be caused by a secondary failure of the bearings, foreign object damage, etc. A high energy disk fragment released at high speed during a disk burst failure is so destructive that it could penetrate the containment ring and damage hydraulic pipelines, electrical and signal cables, oil tanks and airframe, which may lead to the loss of the airplane and passenger fatalities. Although disk burst accidents happen infrequently nowadays, they are unavoidable. Fig.1 shows the CF6-80A2 high pressure turbine disk burst accident that happened at Los Angeles International Airport in June 2006 (Aviation Safety Network, 2006). Moreover, the ability of the case structure to withstand the large dynamic impact and ultimate load generated during a disk burst accident must be considered in the development of new aeroengines. Therefore, it is important to carry out a study of the containment capability of a case impacted by disk fragments.

A number of investigations have included experiments and numerical simulations of projectiles impacting on single and double-layered targets. Almohandes *et al.*(1996) investigated the ballistic resistance of layered steel plates impacted by 7.62 mm diameter standard bullets. They found that a single plate is more effective than layered plates with equal total thickness, and that the impact resistance of layered plates increases as the number of plates decreases and the thickness of the back plate increases. Ben-Dor *et al.*(1998a) presented analytical models for the ballistic resistance of multi-layered ductile targets. They found that for conical-nosed bullets, the ballistic

‡ Corresponding author
* Project (No. 1104-03) supported by the Aviation Propulsion Technology Development Program, China

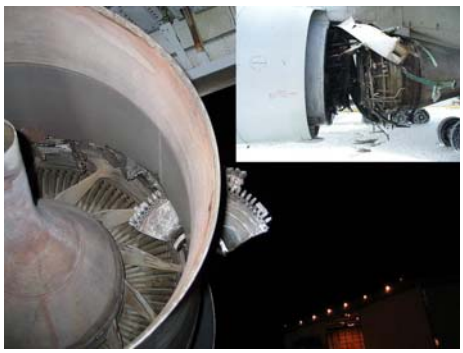

Fig.1 A CF6 Aeroengine turbine disk burst accident

performance of the target is independent of air gap widths and the sequence of the plates in the target. These results were in good agreement with experimental data from Almohandes *et al.*(1996). In a corresponding study, using cylindrical cavity expansion theory, Ben-Dor *et al.*(1998b) concluded that the ballistic limit velocity of the target increases with the increase in widths of the air gaps and the increase of the number of plates in the target, while the total thickness is kept constant. The effect of air gaps on the ballistic perforation resistance of targets was further discussed by Ben-Dor *et al.*(1999). They defined a parameter δ, which determines the effect of an air gap and the order of the plates on the ballistic resistance of the target. If $\delta<0$ then the ballistic limit velocity increases with increasing air gap thickness. However, the ballistic limit velocity does not depend on the air gap width when the air gap thickness becomes more than the length of the impactor. Woodward and Cimpoeru (1998) carried out experiments on layered 2024-T351 aluminum alloy plates impacted by 6.35 mm diameter flat-ended and conical-ended penetrators. They showed that a target system having two plates of equal thickness provided the highest ballistic limit velocity for both nose shapes. In contrast, Zukas and Scheffler (2001) put forward the contrary conclusion. Based on a numerical study, they concluded that layering dramatically weakens thin and intermediate thickness targets. Elek *et al.*(2005) developed an analytical model, which could be used to investigate the impact of a blunt projectile on single and multi-layered spaced targets. According to this developed model, the single layer target has greater resistance than any other multi-layered spaced targets with equivalent total mass. They also found that an increase in the number of spaced layers of a multi-layered target, at constant total mass, causes a further decrease in target resistance. Liang *et al.*(2005) proposed a method for estimating the ballistic limit velocities and residual velocities of multi-layered targets of special bulkheads and shell plating of navy ships, based on several concepts. Their results showed that the ballistic performance is the greatest for a double-layered target when the ratio of the first layer thickness to the total thickness is about 0.75, and that the worse performance occurs when the ratio is 0.5. Dey *et al.*(2007) carried out full-scale impact tests and numerical simulations. They concluded that in the case of blunt projectiles, a larger gain in the ballistic limit velocity is offered by double-layered systems. These advantages seem to disappear when ogival projectiles are used. Gupta *et al.*(2008) studied the effect of projectile nose shape, impact velocity and target thickness on the deformation behavior of layered plates. They found that hemispherical-nosed projectiles require maximum energy for perforation and cause the highest plastic deformation of the target plates. Zhou and Strong (2008) carried out experiments which suggested that for oblique impact by a flat-nosed projectile at angles of obliquity of from 0°~45°, layered plates have a larger ballistic limit than monolithic plates composed of the same material and of the same total thickness, and that for oblique impact by hemispherical-nosed projectiles monolithic plates and layered plates have nearly the same ballistic limit speed.

The above discussion shows that even though different aspects of the problem of projectile impact on layered plates have been studied in previous experiments and numerical simulations, the problem continues to attract research attention. Variations in factors, such as target and projectile geometry, material parameters and impact velocity, have a profound influence on the penetration of the target plates. Different researchers have often used different impact conditions and obtained conflicting results. Therefore, the objective of this paper was to investigate the effect of the standoff distance and thickness pattern of double-layered plates impacted by a disk fragment on ballistic limit velocity using numerical simulation.

In this study, the simulation of phenomena of a 1/3rd disk fragment impact on single and

double-layered plates was carried out using nonlinear dynamical analysis software, MSC.Dytran. The projectile in this study was a disk fragment, unlike in the previous studies. So it is necessary to understand the major failure modes of plates, and to find out the differences in results arising from variations in standoff distance and thickness pattern. This paper consists of four sections. Following this introduction, Section 2 describes numerical models of the disk fragment impact on single and double-layered plates. Section 3 shows the results and analysis of the simulation. The last section presents the conclusions.

NUMERICAL MODELS

A rotating disk usually breaks up into three or four relatively equally proportioned fragments with centrifugal force. The numerical model in this paper assumes a 1/3rd disk fragment. Fig.2 is a sketch of a disk fragment impacting on double-layered plates. The disk has the inner radius R_1=40 mm, outer radius R_2=120 mm, thickness δ=40 mm and the mass of the disk fragment is 12.55 kg. There are two plates of width a=300 mm, length b=800 mm, and with a standoff distance L. Total thickness is h_1+h_2=8 mm for double-layered plates, and h_1=8 mm and h_2=0 mm for single plates. The disk fragment of initial velocity v_0 impacts vertically on the plates, which are set around the four fringe surfaces.

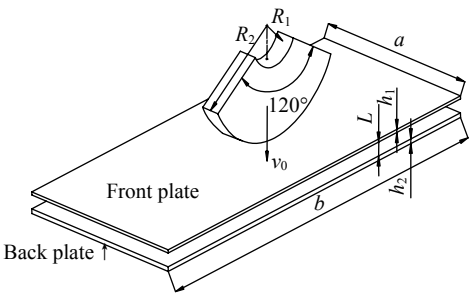

Fig.2 Sketch of disk fragment impacting on double-layered pates

Material modeling

The quality of the material model is a key factor affecting the accuracy of results from a nonlinear finite element simulation, especially of the impact phenomenon. A number of material models are generally used in impact simulation. Due to difficulties in the determination of the material parameters from material tests, simpler models are preferred. In this paper, the Johnson-Cook (JC) model has been used to describe the behavior observed at high velocity impact because it takes into account high strain rate sensitivity, larger deformation, and material softening due to adiabatic heating and damage. The JC model is quite well suited to problems of metal impact and penetration. Moreover, this model is pre-implemented in MSC.Dytran explicit software. According to the explicit formulation of the JC model, the equivalent stress σ_y is defined by

$$\sigma_y=[A+B(\varepsilon^p)^n]\left[1+C\ln\left(\frac{\dot{\varepsilon}^p}{\dot{\varepsilon}_0}\right)\right][1-T^{*m}], \quad (1)$$

where A is the yield stress, B is a constant of material, n is the hardening parameter, C is the strain rate sensitivity and m is the temperature sensitivity parameter. ε^p is the equivalent plastic strain, $\dot{\varepsilon}^p$ is the equivalent plastic strain rate, $\dot{\varepsilon}_0$=1.0 s^{-1} is a reference strain rate, and T^* is the non-dimensional temperature defined as below:

$$T^*=(T-T_0)/(T_{melt}-T_0), \quad T_0\le T\le T_{melt}, \quad (2)$$

where T is the current temperature, T_{melt} is the melting point temperature, and T_0 is the room temperature.

The fracture model proposed by Johnson and Cook (1985) takes into account the effect of stress triaxiality, strain rate and temperature on the equivalent failure strain. The failure criterion is based on the value of the equivalent plastic strain at element integration points. Failure is assumed when a parameter D exceeds unity. The damage parameter D is summed over all increments of deformation, and defined as follows:

$$D=\sum\frac{\Delta\varepsilon_p}{\varepsilon_f}, \quad (3)$$

where $\Delta\varepsilon_p$ is an increment of accumulated equivalent plastic strain that occurs during an integration cycle, and ε_f is the equivalent strain at failure. The strain at failure ε_f, is assumed to be dependent on a non-dimensional plastic strain rate, $\varepsilon^*=\dot{\varepsilon}_p/\dot{\varepsilon}_0$, a

dimension-less pressure-deviatoric stress ratio ($\sigma^*=p/\sigma_{\text{eff}}=-R_\sigma$, where p is the pressure and σ_{eff} is the effective stress) and a non-dimensional temperature T^* as defined previously. The dependencies are assumed separable and take the following expression:

$$\varepsilon_{\text{f}} = (D_1 + D_2 \exp(D_3\sigma^*))(1 + D_4 \ln \dot{\varepsilon}^*)(1 + D_5 T^*) , \quad (4)$$

where D_1, D_2, …, D_5 are failure constants determined from material tests. The model has previously been found to give good results in ballistic penetration problems (Børvik *et al.*, 2005; Dey *et al*., 2007; Gupta *et al*., 2006; 2008). When this failure criterion is met, the deviatoric components of stress are set to zero and remain zero during the rest of the analysis. The element kill algorithm has been used to delete the failed element from the mesh. Thus, using this kind of criterion the mesh in the damaged part must be very fine to not affect the numerical results in terms of energy.

Steel 45 (in the Chinese standard) has been chosen as the material of the disk fragment and plates, since it is often studied and several high strain rate material testing results have been published, which is helpful in obtaining the parameters involved in numerical simulation. The parameters used for the material by Chen *et al.*(2007) are given in Table 1.

Table 1 Parameters used to defined the material and fracture model of steel 45 in the Chinese standard

Parameter	Value	Parameter	Value
ρ (kg/m^3)	7800	T_{melt} (K)	1795
E (GPa)	200	T_0 (K)	300
v	0.3	D_1	0.1
A (MPa)	506	D_2	0.76
B (MPa)	320	D_3	1.57
n	0.28	D_4	0.005
C	0.064	D_5	−0.84
m	1.06		

Finite element model

Taking the symmetry of the model into account, a 1/4th section model was generated in this study. A parameterized solid 3D model is generated in UG software and translated into MSC.Dytran software, whereupon the finite element mesh is defined, and the symmetrical boundary conditions and the constraints on the boundary surfaces are applied. The solid model is meshed using eight-node hexahedron elements and single point integration due to the simplicity of the geometry. The mesh is refined in the impact zone and the mesh density is reduced as the distance from the impact zone increases for computational accuracy and efficiency. Four to eight element layers are taken in the thickness direction. Care is also taken to maintain the correct aspect ratio in the grid, especially in the impact zone where the aspect ratio of the elements is maintained close to unity. The aspect ratio is allowed to increase outside the impact zone. Arbitrary Lagrange-Eulerian method is adopted to describe the impact deformation. Fig.3 shows a finite element model for a 1/4th section model of a disk fragment impacting two layered plates. Some 960 elements for the disk fragment and 6000 elements for the two plates are employed in the analysis. Symmetrical conditions are maintained for the disk fragment and the plates by imposing appropriate displacement constraints on all symmetrical sectional surfaces. Constraints boundary conditions on the marginal surfaces are also applied. Initial velocity is vertically applied to the disk fragment. Surface to surface contact between the disk fragment and the plates is modeled using a kinematic contact algorithm. The fragment is considered as the master surface and the contact surface of the plates as the slave surface, and the contact stiffness scale factor is defined as 1.0. Furthermore, the effect of friction between the disk fragment and the plates is considered. In this work typical values of 0.15 have been defined as the dynamic and static friction coefficients.

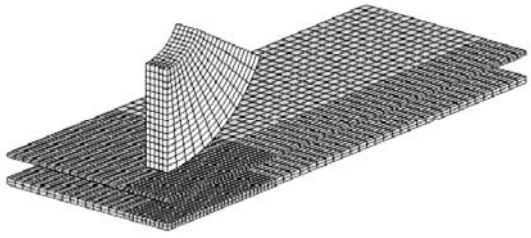

Fig.3 1/4th section finite element model

SIMULATION RESULTS AND ANALYSIS

Analysis of plate impact perforation

The first considerations made during our numerical simulations were to observe the failure mode of single and double-layered plates impacted by a disk fragment. The deformed profiles and von-Mises

stress contours of the disk fragment and a single plate at four different time points are shown in Fig.4. The initial velocity v_0 of the disk fragment in this impact is 172 m/s. It can be seen that prominent bending of the target plate is caused before the shear fracture. During the initial stages of deformation, the largest value of the effective stress is developed at the front side of the plate in the region where the center of the arc edge of the disk fragment contacts the plate. This stress increases with onward movement of the fragment and reaches a peak value at the moment of the shear fracture of the plate. Then the shear fracture spreads from the center to the outside along the arc edge of the disk fragment as it sequentially contacts the plate. A ribbon is sheared out with a width equal to the thickness of the disk. However, the fragment disk pushes and stretches the ribbon, causing the central part of the ribbon to separate from the target plate and fly off at a velocity of 39 m/s. Subsequently, the residual velocity of the disk fragment decreases down to zero at time 2.5 ms. The variation in the total energy E (kinetic energy and internal energy) with the impact time is plotted in Fig.5. The dynamic energy of the disk fragment is absorbed by the plate as the impact process proceeds. After the initial impact, the dynamic energy of the disk fragment hardly decreases, and is mostly converted into the work of plastic and elastic deformation of the plate. At point 1, the plate is penetrated and a special phenomenon occurs. There is a sudden decrease in absorbed energy and then a return to a gradual increase. At point 2, the disk fragment penetrates the plate and the sheared ribbon breaks. The total energy of the plate then reaches and holds a constant value until the end of impact. Meanwhile, the dynamic energy of the disk fragment decreases correspondingly, and falls to zero at the end of impact.

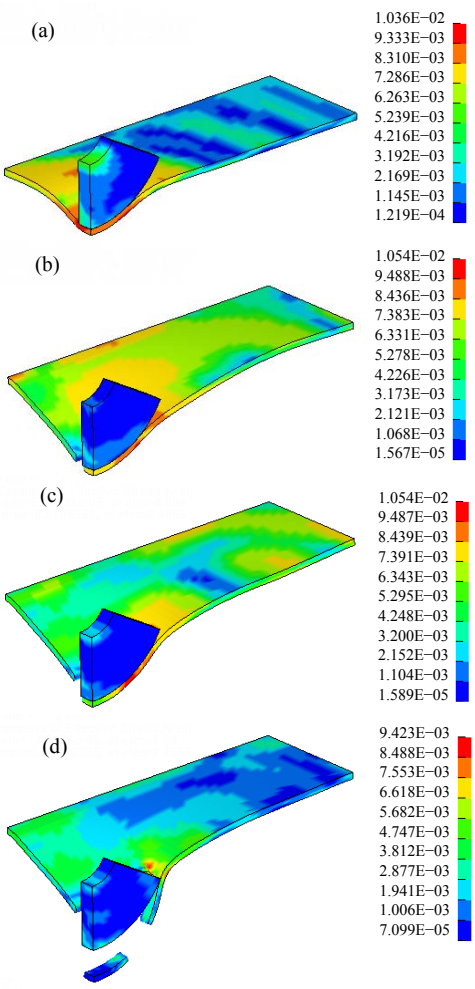

Fig.4 Simulated process of single plate penetration (h_1=8 mm, h_2=0 mm, v_0=172 m/s, unit of the von-Mises stress: 10^5 MPa). (a) Time: 0.32 ms; (b) Time: 0.80 ms; (c) Time: 1.12 ms; (d) Time: 2.50 ms

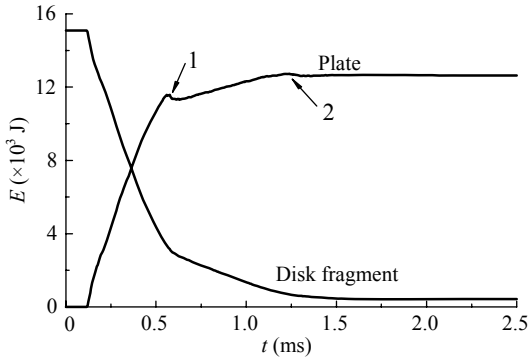

Fig.5 Variation in total energy with time of single plate impact (h_1=8 mm, h_2=0 mm, v_0=172 m/s)

The deformed profiles and von-Mises stress contours at four different time points of a disk fragment impact on double-layered plates are shown in Fig.6, where h_1=4 mm, h_2=4 mm, L=20 mm and v_0=160 m/s. Fig.7 shows the total energy (kinetic energy and internal energy) change of the disk fragment and the two plates. Each plate suffers a failure process similar to that of a single impacted plate in the case above. The plates first suffer large bending deformation, then shear failure along the edge of disk fragment contacting the plate. A ribbon forms and breaks off in the center of the impacted zone. At point 1, the front plate is perforated. At the time, damage to

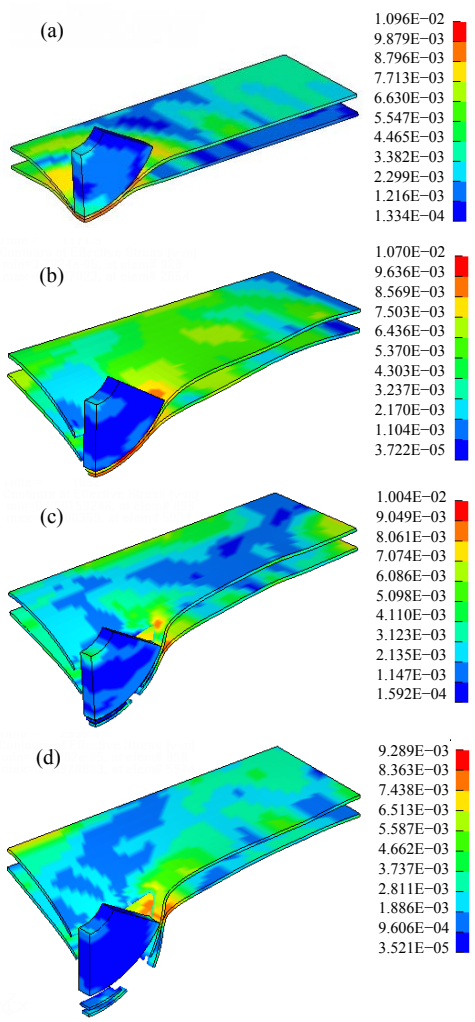

Fig.6 Simulated process of double-layered plate penetration (h_1=4 mm, h_2=4 mm, L=20 mm, v_0=160 m/s, unit of the von-Mises stress: 10^5 MPa). (a) Time: 0.40 ms; (b) Time: 1.17 ms; (c) Time: 1.89 ms; (d) Time: 3.00 ms

the back plate is dominated by membrane stretching while the front plate suffers plate bending and shearing. After perforation by the disk fragment, the two layers of the target plate are found to be in direct contact with each other. This may be due to the fact that the layered plates impacted by the disk fragment remain in contact till the end of the perforation phenomenon. As shown in Fig.7, because of perforation the energy of the front plate increases slowly, while the energy of the back plate increases rapidly. Similarly, after the back plate is perforated at point 2, its energy also increases slowly. It is clear that the energy absorbed by the back plate is larger than that by the front plate, because more bending plastic deformation is caused in the back plate than in the front plate. Finally, the disk fragment wastes all dynamic energy and stops moving or may be captured in the center of the perforated hole on the plates, and two plate fragments fly off at a velocity of 24 m/s.

Ballistic limit velocity

To analyze the influence of plate distance and thickness configurations, ballistic limit velocity v_{b1} under different conditions is presented. Variation in the ballistic limit velocity when the spacing distance L between two plates ranges from 0 to 32 mm is shown in Fig.8. In this case, the thickness of each of the two plates is 4 mm. When L<9 mm, ballistic limit velocity decreases with spacing distance; when 9 mm<L<28 mm, ballistic limit velocity increases with spacing distance; when L>28 mm, ballistic limit velocity decreases with the spacing distance again. Fig.9 shows a

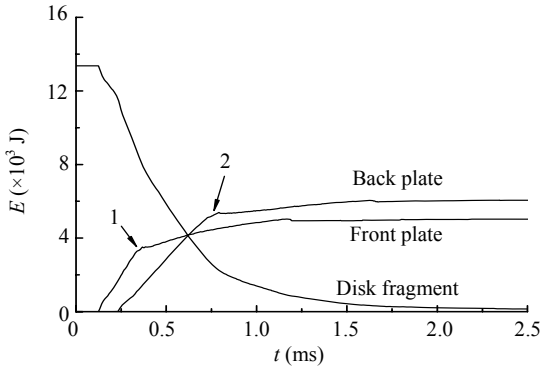

Fig.7 Variation in total energy with time of double-layered plate impact (h_1=4 mm, h_2=4 mm, L=20 mm, v_0=160 m/s)

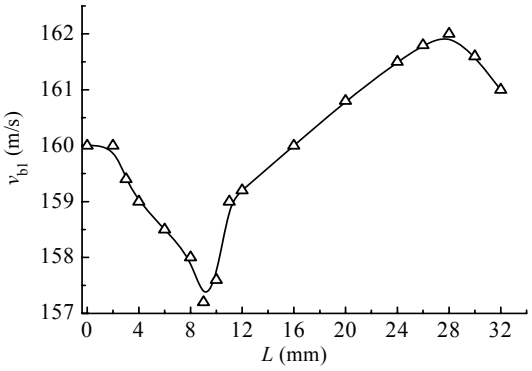

Fig.8 Ballistic limit velocity versus spacing distance between double-4 mm-thickness-layered plates

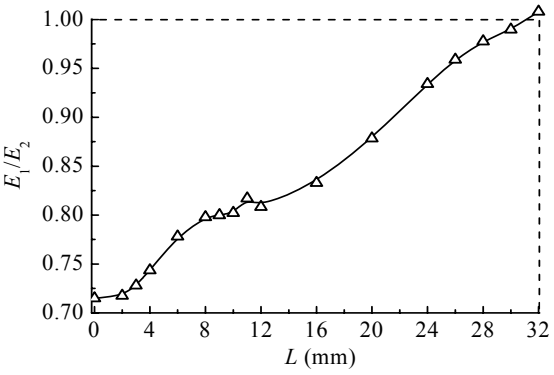

Fig.9 Ratio of energy absorbed by the front and back plates versus spacing distance

sketch of the ratio of energy E_1/E_2 absorbed by the front and back plates, each with a thickness of 4 mm, versus different spacing distances. E_1/E_2 increases with the spacing distance between layers, and when the spacing closes to a certain value L=31 mm the ratio reaches 1.0. Fig.8 also shows that the largest resistance point occurs slightly before the ratio of energy absorbed by the two plates reaches 1.0. Resistance of the double-layered plates decreases as the ratio is larger than 1.0.

Variation in ballistic limit velocity with space distance when the thicknesses of the front and back plates is 2 and 6 mm, respectively, is shown in Fig.10, and is clearly different from that shown in Fig.8. There is no orderliness when L<16 mm, and the ballistic limit velocity increases as the spacing distance increases when L>16 mm. When L>32 mm the ballistic limit velocity greatly increases with spacing distance.

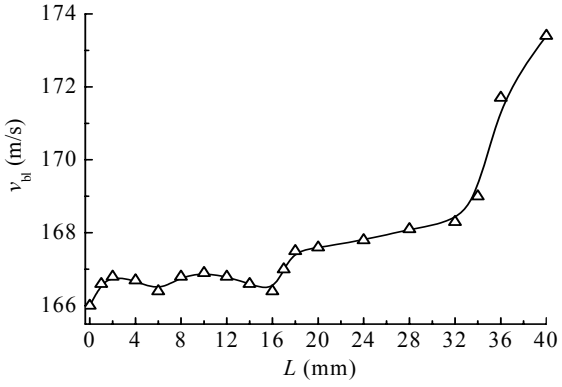

Fig.10 Ballistic limit velocity versus spacing distance between the double-layered plates with h_1=2 mm, h_2=6 mm

Variation in ballistic limit velocity with the thickness ratio p of the front plate is shown in Fig.11, with a constant total thickness of h_1+h_2=8 mm and a spacing distance between the two layers of L=16 mm. When p=0 and p=100% for convenience of comparison, the results of a single plate with a thickness of 8 mm are shown. Ballistic limit velocity decreases as p increases at first, then when p is larger than 50% the ballistic limit velocity increases. A single plate has the greatest resistance, and when p is smaller or larger the resistance is greater. However, when the thickness of the two plates is similar, the plates have the least resistance.

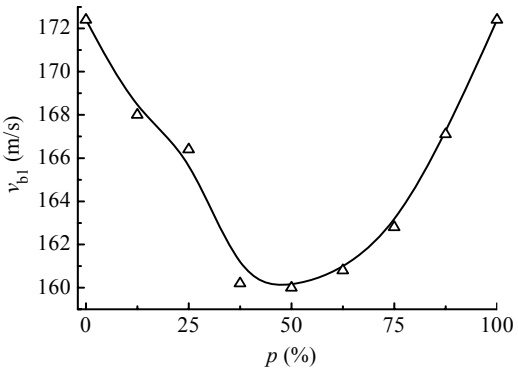

Fig.11 Ballistic limit velocity versus thickness ratio of the front plate

Comparing Figs.10 and 11, we find that the ballistic limit velocity is 173.4 m/s when the spacing distance is 40 mm, and is greater than 172.4 m/s in the single plate case (p=0 or p=100%). Thus, the resistance of double-layered plates may exceed that of a single plate with equal total thickness if the thickness ratio and standoff distance between the double-layered plates are set appropriately.

CONCLUSION

Finite element simulations of a disk fragment impact on single and double-layered plates were carried out. The explicit finite element code MSC.Dytran in conjunction with the JC material model was used to consider the effect of strain rate. Based on the simulation observations presented, the following conclusions were drawn:

(1) The main failure modes of plate are bending,

shearing and tensile fracture in the impacted zone.

(2) The ballistic limit velocity of double-layered plates with each layer of equal thickness increases with the spacing distance between layers, as long as the spacing distance is moderate.

(3) Resistance appears different for different thickness patterns of the two plates. When the thickness ratio of the front plate is smaller or larger than 50%, the resistance is greater.

(4) A single plate target has greater resistance than a double-layered plate target when the thickness of each layer is half that of a single plate. However, the resistance of a double-layered plate can exceed that of a single plate with the same total thickness if the plates are arranged appropriately.

References

Almohandes, A.A., Abdel-Kader, M.S., Eleiche, A.M., 1996. Experimental investigation of the ballistic resistance of steel-fiberglass reinforced polyester laminated plates. *Composites Parts B: Engineering*, **27**(5):447-458. [doi:10.1016/1359-8368(96)00011-X]

Aviation Safety Network, 2006. Aircraft Accident Boeing 767-223 ER N330AA Los Angeles International Airport [EB/OL]. Available from: http://aviation-safety.net/database/record.php?id=20060602-0 [Accessed 17/02/2008]

Ben-Dor, G., Dubinsky, A., Elperin, T., 1998a. On the ballistic resistance of multi-layered targets with air gaps. *International Journal of Solids and Structures*, **35**(23):3097-3103. [doi:10.1016/S0020-7683(97)00358-2]

Ben-Dor, G., Dubinsky, A., Elperin, T., 1998b. Effect of air gaps on ballistic resistance of target for conical impactors. *Theoretical and Applied Fracture Mechanics*, **30**(3):243-249. [doi:10.1016/S0167-8442(98)00059-7]

Ben-Dor, G., Dubinsky, A., Elperin, T., 1999. Effect of air gap and order of plates on ballistic resistance of two layered armor. *Theoretical and Applied Fracture Mechanics*, **31**(3):233-241. [doi:10.1016/S0167-8442(99)00017-8]

Børvik, T., Clausen, A.H., Eriksson, M., Berstad, T., Hopperstad, O.S., Langseth, M., 2005. Experimental and numerical study on the perforation of AA6005-T6 panels. *International Journal of Impact Engineering*, **32**(1-4):35-64. [doi:10.1016/j.ijimpeng.2005.05.001]

Chen, G., Chen, X., Chen, Z.F., Qu, M., 2007. Simulation of A3 steel blunt projectile impacting 45 steel plates. *Explosion and Shock Waves*, **27**(5):390-397 (in Chinese).

Dey, S., Børvik, T., Teng, X., Wierzbicki, T., Hopperstad, O.S., 2007. On the ballistic resistance of double-layered steel plates: An experimental and numerical investigation. *International Journal of Solids and Structures*, **44**(20):6701-6723. [doi:10.1016/j.ijsolstr.2007.03.005]

Elek, P., Jaramaz, S., Micković, D., 2005. Modeling of perforation of plates and multi-layered metallic targets. *International Journal of Solids and Structures*, **42**(3-4):1209-1224. [doi:10.1016/j.ijsolstr.2004.06.053]

Gupta, N.K., Iqbal, M.A., Sekhon, G.S., 2006. Experimental and numerical studies on the behavior of thin aluminum plates subjected to impact by blunt- and hemispherical-nosed projectiles. *International Journal of Impact Engineering*, **32**(12):1921-1944. [doi:10.1016/j.ijimpeng.2005.06.007]

Gupta, N.K., Iqbal, M.A., Sekhon, G.S., 2008. Effect of projectile nose shape, impact velocity and target thickness on the deformation behaviors of layered plates. *International Journal of Impact Engineering*, **35**(1):37-60. [doi:10.1016/j.ijimpeng.2006.11.004]

Johnson, G.R., Cook, W.H., 1985. Fracture characteristics of three metals subjected to various strains, strain rates, temperatures and pressures. *Engineering Fracture Mechanics*, **21**(1):31-48. [doi:10.1016/0013-7944(85)90052-9]

Liang, C.C., Yang, M.F., Wu, P.W., Teng, T.L., 2005. Resistant performance of perforation of multi-layered target using an estimation procedure with marine application. *Ocean Engineering*, **32**(3-4):441-468. [doi:10.1016/j.oceaneng.2004.05.009]

Woodward, R.L., Cimpoeru, S.J., 1998. A study of the perforation of aluminium laminate targets. *International Journal of Impact Engineering*, **21**(3):117-131. [doi:10.1016/S0734-743X(97)00034-1]

Zhou, D.W., Strong, W.J., 2008. Ballistic limit for oblique impact of thin sandwich panels and spaced plates. *International Journal of Solids and Structures*, **35**(11):1339-1354. [doi:10.1016/j.ijimpeng.2007.08.004]

Zukas, J.A., Scheffler, D.R., 2001. Impact effects in multi-layered plates. *International Journal of Solids and Structures*, **38**(19):3321-3328. [doi:10.1016/S0020-7683(00)00260-2]